The Acoustic Emission from Asperity Interactions in Mixed Lubrication

S. Hutt, A. Clarke*, R. Pullin , H.P. Evans.

School of Engineering, Cardiff University, Cardiff, United Kingdom.

*corresponding author, clarkea7@cardiff.ac.uk

Abstract

Gears typically operate in mixed lubrication conditions, where the lubricant film is too thin to prevent opposing surface asperities from interacting with each other. The likelihood / intensity of interactions is indicated by the Λ ratio: the ratio of film thickness to surface roughness. Researchers have asserted that asperity interactions are the predominant cause of Acoustic Emission (AE) in healthy gear contacts. However direct experiments on gears have yet to yield a clear relationship between the Asperity AE (AAE) and Λ ratio, this is in part due to the complexity of gear tooth contacts. In this paper a disk rig was used to simulate a simplified gear contact so that the fundamental relationship between AAE and Λ could be investigated more effectively. By varying oil temperature and entrainment speed a wide spectrum of lubrication conditions was generated. In contrast to other published studies an independent measurement technique, the Contact Voltage (CV), was used to verify the amount of interactions, and repeated roughness measurements were used to confirm minimal surface wear. A simple, consistent and precise relationship between AAE amplitude and Λ was identified and defined for changes from full-film to mixed lubrication. Within the mixed lubrication regime, the AAE amplitude increased exponentially as Λ decreased at all speeds tested. It was also observed that an increase in speed always resulted in an increase in AAE amplitude, independently of any changes in Λ. This direct effect of speed was modelled so that the AAE could be predicted for any combination of speed and Λ within the tested envelope. This paper links gear contact tribology and AE with new precision and demonstrates the potential of using AAE as a sensitive monitoring technique for the lubrication condition of gears.

Keywords: Acoustic Emission; Asperity interactions; Mixed lubrication; Gears; EHL

1 Introduction

Acoustic Emission (AE) refers to the elastic waves that are naturally released by, and propagate through, dense (non-gaseous) materials. AE is localised and is caused by various micro-mechanical mechanisms such as crack growth and changes to the crystal structure in metals, and by cavitation and turbulence in fluid flow [1]. AE measurement is well-established as a tool for condition monitoring and non-destructive testing of static structures, for example detecting the location of flaws in pressure vessels. This paper is concerned with using AE to study conditions in machine parts such as gear contacts where both rolling and sliding motion and significant effects of surface roughness occur.

Recent attempts have been made to detect incipient damage and adverse operating conditions in gears by analysis of their AE 'signature'. Some of this research takes the pragmatic view that a full understanding of the fundamental sources of AE from gears is unnecessary: all that is required is to show that some AE parameter changes from a healthy gear to a damaged one. Using this approach researchers have shown on laboratory test rigs that AE measurements can detect artificially seeded (spark eroded) surface defects with greater sensitivity than vibration measurements [2], and that they can also detect tooth crack propagation and tooth loss more effectively [3–5]. The limitation of this healthy vs. damaged characterisation is that it is difficult to quantify the results in such a way that they can be extrapolated beyond the parameters of the specific experiment.

In contrast to direct tests on real-world components some tribologists have investigated the nature of AE from a variety of more idealised, or basic, moving contacts. For example Asamene and Sundaresan [6] measured the AE from unlubricated pads moving in a stick-slip cycle (the contact geometry was analogous to that of a rotor between brake pads). They found that AE occurred predominantly in the slip cycle and this was attributed to numerous collisions between opposing roughness asperities. They also identified signal characteristics that varied systematically with changes to the contact pressure, sliding speed and surface roughness. Using a micro-scale pin-on-block geometry, Hase *et al.* [7] determined that changes to the spectral content of the AE signals allowed discrimination between adhesive and abrasive wear mechanisms. Testing a lightly loaded ball-on-cylinder geometry, Benabdallah and Aguilar [8] found that for dry contacts, the AE amplitude had a correlation with friction and wear rate; and for grease lubricated contacts, a coarse dependence on the film thickness. There is now a sufficiently diverse body of work to suggest that in general, any interactions between opposing roughness asperities in moving contacts will be a source of AE, here this is termed AAE (Asperity Acoustic Emission) to distinguish it from more general AE.

Gear tooth contacts can be lubricated effectively because of the elastohydrodynamic mechanism. This entrains a film of highly pressurised, and therefore viscous, oil between the two 'contacting' surfaces. The oil film, if thick enough, can separate the surfaces to the extent that their roughness has no significant effects on the contact, and this is termed 'full-film' lubrication. However, in many practical applications the surfaces have roughness asperities of a similar scale to the oil film thickness and it is possible for opposing asperities to interact, this is termed 'mixed' lubrication. An interaction may be a 'close-pass' whereby the oil film maintains a marginal separation between passing asperities but is extremely thin and can have a large local pressure spike. Alternatively, an interaction may involve local rupture of the oil film and direct contact between asperities, i.e. a localised incidence of boundary lubrication. Mixed lubrication is a spectrum within which the number and severity of asperity interactions can vary depending on the precise surface and operating conditions. Gear surfaces operating in mixed lubrication are at risk of damage from wear mechanisms such as micropitting [9,10] and

therefore methods to measure the amount and severity of asperity interactions are of great interest for health monitoring purposes.

The propensity for asperity interactions is typically indicated by the Lambda ratio, Λ, (also known as the specific film thickness). First proposed by Tallian [11], this is defined as

$$\Lambda = \frac{h}{R_C} = \frac{h}{\left({R_{qA}}^2 + {R_{qB}}^2\right)^{1/2}} \quad (1)$$

where h is the film thickness for an equivalent contact with smooth surfaces, and R_C is the composite roughness. R_C is composed of R_{qA} and R_{qB}, which are the R_q (RMS roughness) of the two surfaces. Λ is a measure of the inherent film forming capability of the lubrication mechanism taking into account load and temperature variation, with decreasing Λ values indicating decreasing film forming capability. Λ is a widely used parameter in the tribological consideration of rough surfaces and has been shown to correlate with gear and bearing fatigue life [12]. It is also an active factor in ISO and AGMA gear design standards. As such Λ is a useful and widely accepted parameter, which it is helpful to establish by independent measurement. AE provides a practical route to achieve such measurements. Several established laboratory techniques are already available, such as optical interferometry [13] and electrical resistance measurements [14] but these cannot easily be applied in the field. Measuring the AAE potentially offers a more practical way to determine the lubrication conditions in real-world gears.

Some researchers have sought to identify AAE from gears directly, i.e. using actual gear contacts, but this is difficult due to the inherent complexity of gear contacts. The oil film thickness, and therefore Λ, varies not only with the global operating conditions (e.g. speed, torque and temperature) but also locally over the tooth contact cycle due to variations in geometry, kinematics and load sharing between teeth. For healthy spurs gears operating in steady state conditions, the observed AE is typically continuous but with transient spikes in amplitude, occurring at the frequency of the tooth contact cycle [15–17]. Researchers at Cranfield University, who have undertaken a variety of experiments directly on gears, concluded that the AE is predominantly caused by asperity interactions and that the pure rolling conditions at the pitch point are responsible for the transient spikes [16,17]. However they offer no explanation as to how the state of pure rolling causes AE of higher amplitude than rolling/sliding conditions away from the pitch point. Additionally there are other possible sources of AE in gears such as tooth resonance [17], the outlet pressure spike associated with EHL [17], and the shock loading caused by tooth engagement [15] which have not been fully investigated.

As well as investigating the fluctuations in AE over the tooth contact cycle, the Cranfield researchers have also investigated the effects of changes in the global operating conditions. Testing different steady state combinations of speed and torque, Raja Hamzah and Mba [16] found that as Λ decreased the AE_{RMS} (the RMS of the AE) increased linearly. In another experiment Raja Hamzah *et al.* [18] used temperature control to induce large scale changes in the oil film thickness. For both spur and helical

gears, two different lubricants, and six different combinations of torque and speed were studied, and liquid nitrogen was used to cool the gears to 0 °C before allowing them to passively reheat. For the helical gears the relationship between Λ and the AE_{RMS} during the reheating was inconsistent, however for the spur gears, the AE_{RMS} consistently increased as Λ decreased to values which typically indicate mixed lubrication. Unfortunately the apparent relationship between Λ and the AE_{RMS} differed considerably depending on the specific combination of speed, torque and lubricant tested. For some combinations the AE_{RMS} increased only slowly, if at all, until a low Λ threshold was reached, after which it increased seemingly exponentially. But for other conditions there was no threshold, instead the increase was more gradual and occurred from high Λ values. Although the results of these experiments show that AE increases in-line with the probability of asperity interactions it is unclear how well their Λ values relate to the precise contact conditions; Λ was calculated on the assumption of constant roughness, i.e. no wear, and there is no explanation of how the calculation accounts for film-thickness variations over the tooth contact cycle.

To further complicate matters the Cranfield researchers [16–18] and others [15,19] have found that increasing the speed of gears dramatically increases the amplitude of AE *despite* the corresponding increase in Λ which should cause any AAE to decrease. In other words, the speed has a direct effect on the AE independent of its effect on Λ. This 'direct speed effect' has, as yet, no established explanation. Some have attributed it to the increased strain rate of asperity interactions [17], however it has also been observed in experiments on both rolling element and plain bearings operating in full-film conditions [20,21] so it must have other causes as well.

Although it is apparent that, in general, the amplitude of AE from gears increases as Λ decreases, to date no experiments have established a precise and coherent relationship between Λ and AAE in mixed lubrication. This paper seeks to rectify this by using a disk rig to simulate a simplified gear contact, and by validating the amount of asperity interactions by direct measurement. As demonstrated by Merritt [22] the contact geometry and kinematics for any point in the gear tooth contact cycle can be approximated by an equivalent contact between two disks (rollers). Contact between two disks can replicate, continually and in steady state, an instantaneous moment in the gear tooth contact cycle. Advantages of testing on disks as opposed to gears are that more of the contact parameters can be set as constants, there are no continual start/stop effects due to tooth engagements and disengagements, and surface measurements are easier as the flanks of gear teeth are difficult to access. The disk rig used for this work can generate a contact having a load, area, motion and roughness equivalent to a gear tooth contact, and is also instrumented so that the precise lubrication conditions of the contact can be determined. It represents a good compromise between realism and simplicity, bridging a gap between condition monitoring experiments on real systems and tribological investigations on small scale micro-contacts. Using this rig, the experiments presented in this paper uncover the relationship between Λ and

AAE in new detail and it is envisaged that this will prove useful for those seeking to use AE measurements for condition monitoring of gears and for mixed lubrication contacts more generally.

2 Test Method

2.1 The disk rig

Figure 1 shows a schematic of the rig. The test disks are driven by an interchangeable helical gear pair, the ratio of which determines the sliding/rolling ratio (SRR) of the test contact. The fast shaft is supported by fixed bearings and the slow shaft by bearings in a pivoting housing. This allows the slow disk to move towards and away from the fast disk in response to the load. A hydraulic ram is used to apply the load and when the ram is unpressurised, the disks are separated to allow the rig to be run up to speed before the test contact is made. The rig is driven by a variable frequency electric motor geared to give fast shaft speeds of 200 – 2000 rpm. An encoder on the fast shaft provides a pulse once per rotation and this is used to synchronise all measurements.

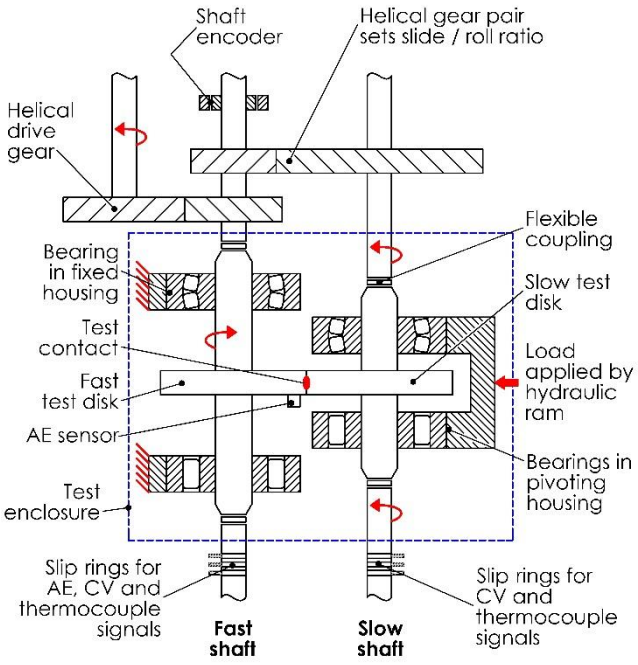

Figure 1. Schematic of the disk rig.

For this work the rig was lubricated by a naval gear oil with extreme pressure additives, conforming to Defence Standard OEP-80 [23]. It is pumped from a temperature controlled tank to a manifold which supplies the test contact, drive gears and support bearings. Jets are positioned directly on the inlet and outlet of the contact to ensure it is always flooded. The temperatures of both disks are measured using thermocouples embedded 3 mm below their contact surfaces. These temperature signals are routed

through slip rings at the ends of the two shafts. The temperature of oil at the inlet of the contact is also measured using a thermocouple attached to the jet nozzle.

The disk rig is instrumented to provide an electrical resistance-based measurement of the amount of asperity contact. To facilitate this, the slow disk is electrically isolated from the body of the rig using a combination of ceramic bearing elements and polymeric couplings. A potential divider circuit measures the potential between the disks, termed here the Contact Voltage (CV). The lubricated contact is analogous to a variable resistor placed across the disks. In full film lubrication, when the oil film fully separates the disks, the contact resistance is essentially infinite and the CV will be at a maximum. In boundary lubrication, the number of direct asperity contacts is sufficient to provide a continual conduction path through the oil film and the contact resistance and CV is at a minimum. In mixed lubrication conditions the contact resistance fluctuates rapidly with the instantaneous amount of direct asperity contacts, and the CV takes intermediate values accordingly [14]. Continuous and high frequency CV signals, termed here CVc, reveal the rapid fluctuations associated with the progression of asperities through the contact. Mean CV measurements (over time), termed here CVm, indicate the lubrication regime. For the experiments presented in this paper the potential divider circuit was calibrated so that the maximum CV was 44 mV. For ease of interpretation, all CV results (CVc and CVm) presented here are normalised so that 0 is the minimum and 1 is the maximum (full film conditions). A more detailed description of the CV technique used on the disk rig can be found in [14].

2.2 The test disks

The test disks have a diameter of 76.2 mm, width of 9.5 mm and a slight crown with a radius of 304.8 mm. When loaded an elliptical contact area is generated with the minor axis aligned in the direction of rotation, and an aspect ratio of 3.91 to 1. Testing a long and thin elliptical contact is preferable to testing a linear (roller) contact as it avoids uncontrolled end effects caused by geometric discontinuity, (i.e. the edges of the disks) and is self-aligning. The long, thin ellipse simulates the contact of gear teeth with axial crowning relief.

The disks used for this paper were made of a gear steel, Rolls-Royce 6010, and were case hardened. They were crowned using a special grinding technique [24] which gives a roughness topography with a lay and direction of motion similar to that of common helical gear teeth. The roughness topography of the disks consists of slightly curved ridges and valleys running transversely to the direction of motion. Figure 2 shows the roughness topography of the fast and slow disks individually within the Hertzian contact and the composite roughness topography that results when the disks are in their assembled orientation. The individual disk topographies curve in opposing directions which results in a cross-hatched composite topography, i.e. the ridges and valleys of each disk intersect those of the other at a shallow angle.

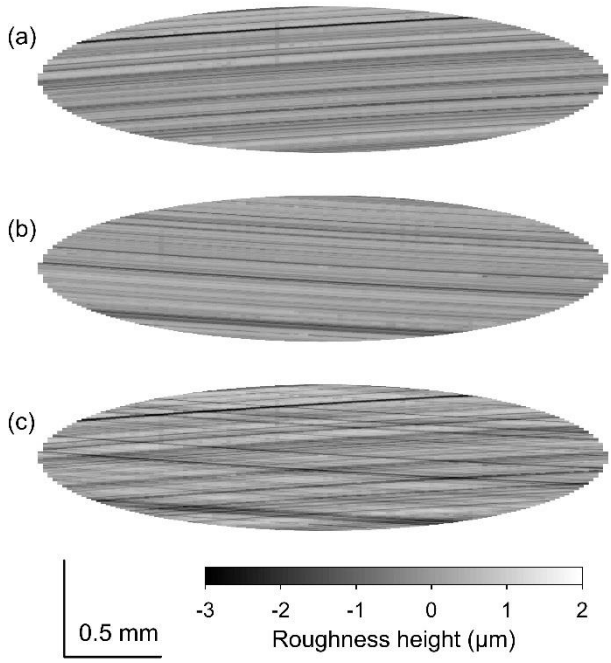

Figure 2. The ground roughness topography as orientated in the contact for (a) the fast disk, (b) the slow disk and (c) their composite (sum) roughness. The direction of surface motion is upwards (for both disks). The area shown corresponds to a maximum Hertzian pressure of 1.2 GPa.

Two pairs of disks were used for the experiments presented in this paper. For one pair the disks surfaces were left as-ground (as shown in Figure 2). For the other pair, the surfaces were smoothed using an isotropic superfinishing process. These two disk pairs are termed 'rough' and 'smooth' respectively. Prior to the experiments presented here the rough disk pair had been used extensively to investigate the AAE from running-in and so the surfaces had the typical post running-in characteristics: a negatively skewed roughness profile with flattened and rounded asperities. The effects of running-in on similar disks have been investigated previously and are described in detail in [19]. The smooth disk pair had not been tested previously. Table 1 gives the Vickers hardness and R_q of the disks at the start of testing.

Table 1. The hardness and roughness of the disks prior to testing.

	Vickers hardness	R_q (RMS roughness) (μm)
Rough fast disk	760	0.37
Rough slow disk	765	0.35
Smooth fast disk	735	0.067
Smooth slow disk	740	0.064

2.3 Acoustic emission instrumentation

Useful AE is typically very high frequency, 10s to 1000s of kHz, and attenuates rapidly with distance and across mechanical interfaces. Thus the choice of sensor position provides some means to selectively detect the AE from a specific component. It was decided to position a sensor on the fast disk as this favours detecting AE from the relatively close test contact, rather than the relatively far-away bearings and gears. In another experiment by the authors [25] an additional sensor was placed on one of the support bearing housings. It was found that the amplitude of AE at this site was an order of magnitude less than that at the fast disk. So when the additional attenuation distance / interfaces are taken into account it is extremely unlikely that any AE from the bearings, or even more distant gears, is of significant amplitude if it reaches the sensor on the fast disk.

The sensor used to measure the AE was a Physical Acoustics Pico sensor. This type of sensor has a nominal operating range of 200 – 750 kHz and a resonant frequency of 250 kHz. It was selected primarily for its small size rather than frequency characteristics: the rig was not originally designed for AE instrumentation and consequently there was little space near the test contact within which to add a sensor. The sensor was clamped directly to the side of the fast disk near its outer edge. A silicone sealant was used as an acoustic couplant (to aid transmission across the disk / sensor interface) and a slip-ring was used to connect the sensor to the AE acquisition system. The signal was conditioned by a pre-amplifier with a gain of 40 dB and a 20 kHz highpass filter. The 20 kHz highpass filter helped ensure that vibrational frequencies associated with the various rotating components of the rig were not measured. (For example the highest gear mesh frequency for the procedure used in this paper was approximately 6 kHz). A dedicated Physical Acoustics computer was used to perform the Analogue to Digital Conversion (ADC) on the signal and save it when triggered by the rig computer.

2.4 Test parameters

The test parameters and procedure were designed to generate a wide range of lubrication conditions from full-film to well within the mixed regime with the rough disk pair. Testing on the smooth disk pair was only intended to provide full-film control data for comparative purposes. It was decided to effect different lubrication conditions by varying the entrainment velocity (disk rotational speed), and the oil viscosity by means of its temperature. The load was not chosen as a variable as this primarily affects contact area rather than the lubrication conditions. The SRR was also kept constant so that the specific composite roughness topography, i.e. which specific opposing asperities met in the contact, was also constant. The values of the constant parameters are given in Table 2.

Table 2. Constant contact parameters

Slide / roll ratio, [Gear ratio]	0.5, [5/3]
Load (calibrated at 100°C) (N)	1460
Maximum Hertzian contact pressure (GPa)	1.2
Hertzian contact dimensions (mm)	0.77 × 3.01

Because of the anticipated direct speed effect it was decided to vary the speed in discrete steps so that changes to the AE caused by this could easily be discriminated from those of changing lubrication conditions. For each discrete speed, the lubrication conditions were made gradually more severe by continual heating of the lubricating oil. Temperature induced changes to material properties, geometry and sensor characteristics can affect the observed AE [26], however there is no evidence that these effects are significant in comparison to changes caused by the lubrication conditions [18].

2.5 Test sequence

For consistency it was desirable to minimise the amount of surface modification during testing. So prior to the main experimental programme, the test contact was operated for a short period at lubrication conditions more severe than any subsequently used. This ensured that any running-in of asperities would occur in this pre-conditioning stage and not in subsequent tests. Table 3 presents the test sequence for both disk pairs. For the pre-conditioning, test stage 0, the rig was preheated by circulating hot lubricating oil for several hours until the temperature of the test enclosure was raised to near that of the oil bath. The disks were then loaded and run at slow speed for several minutes. For the main test stages, 1 to 5, the rig was cold started as follows: With the oil bath and test enclosure at ambient lab temperature the lubricant pump was started and the rig run up to speed. Once at speed, data acquisition commenced and then the load was applied to start the test. At this time the oil bath heater was switched on and rig allowed to run until the oil bath temperature reached ~110°C.

Table 3. Test sequence

Test Stage	Mean entrainment speed, $\bar{u}$ (m/s)	Oil bath temperature (°C)
0 (Pre-conditioning)	0.64	110
1	0.96	Ambient – 110
2	1.60	Ambient – 110
3	3.19	Ambient – 110
4	4.79	Ambient – 110
5	6.38	Ambient – 110

2.6 *Sampling regime*

The AE and CVc were sampled every 25th rotation of the fast disk for a period of one rotation. For the SRR of 0.5 the specific composite roughness has a length of five fast disk rotations, i.e. the same opposing roughness features meet every 5th fast disk rotation. Using an acquisition interval that was a multiple of five ensured that sampling was synchronised with the specific composite roughness, which was desirable for consistency. For testing on the rough disks the ADC rate was 5 MHz, and for the smooth disks 2 MHz, (an additional ancillary sensor was added to the rig for the smooth disk tests and hardware limitations necessitated the decrease in ADC rate). Other rig measurements: temperature, load, speed, and CVm, were sampled and averaged for every fast disk rotation.

2.7 *Surface measurements*

Surface profile measurements were made in-situ (with the disks assembled in the rig) using a portable Taylor Hobson 2D profilometer. Due to the nature of mixed lubrication some wear was anticipated, and so for the rough disks measurements were taken before and after each test stage. The smooth disks were not expected to generate severe mixed lubrication conditions and so for these, measurements were only taken before and after the pre-conditioning test stage, and then at the end of the entire test sequence. The measurements were repeated at precisely specified disk positions so that the wear history of specific surface features could be recorded. The procedure used to make repeat position in-situ profile measurements is described in detail in [25]. For each disk, measurements were made on the centre-line of the contact path and at three circumferential positions. The length of each profile was 12 mm. The roughness profiles were extracted from the broadband surface measurements using a Gaussian filter with a 0.8 mm cut-off This cut-off was chosen as it corresponds to the length of the contact in the entrainment direction. The R_q of each individual profile was then calculated.

2.8 *Calculation of the film thickness and Λ.*

The central smooth surface film thickness h_c was chosen as the representative film thickness parameter. h_c is the film thickness at the central parallel region of a smooth surface EHL contact, as opposed to h_m which is the minimum film thickness which occurs at the constriction [27]. h_c was calculated using the appropriate CDDT formula, in this case the variant for entrainment in the direction of the minor axis of a contact ellipse [27]:

$$H_c = \frac{h_c}{R_x} = 4.30(U^{0.68})(G^{0.49})(W^{-0.073})\left\{1 - exp\left(-1.30\left(\frac{R_y}{R_x}\right)^{2/3}\right)\right\} \quad (2)$$

where H_c and h_c are the dimensionless and dimensional central film thickness; U, G and W are the dimensionless groups representing respectively the influence of speed, material and load; and R_x and R_y are the effective radii of curvature of the contact bodies. The measurements of the disk temperatures, load and speed taken during the test procedure (in conjunction with temperature-pressure-viscosity data

for the oil, the disk geometry and elastic modulus) allowed h_c to be calculated for each fast disk rotation. (Note: it should be emphasised that at points in the test procedure where surface roughness was significant, h_c does not indicate the actual conditions but those that would have been expected had the surfaces been smooth).

Finally Equation (1) was used to calculate Λ for each fast disk rotation using h_c and R_C. For each test a constant value of R_C was used which was the average of the R_q measurements taken before and after the test.

3 Results and discussion

The results and discussion are structured as follows. First the results used to calculate Λ (the surface roughness, temperature, load and h_c) are presented and discussed in Sections 3.1 and 3.2. Then the Λ results are introduced in Section 3.3, and compared against the contact voltage measurements in Section 3.4 to verify the lubrication conditions. Then AE measurements from the rough disk pair are presented Section 3.5 and analysed in relation to the known lubrication conditions. Finally a comparison between the AE from the rough and smooth disks is made in Section 3.6.

3.1 Surface roughness

Figure 3 shows the R_q of each disk vs. the progress through the test schedule. Each R_q value shown is the mean from the three circumferential positions sampled on each disk. For the rough disk pair the R_q of the un-run surfaces is also shown for comparison. (The smooth disk pair had not been used for prior testing so the measurement taken before test stage 0 is the un-run surface).

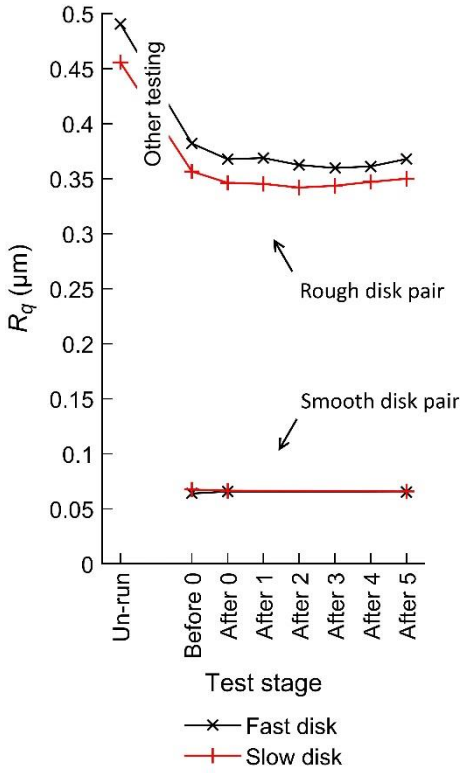

Figure 3. R_q measurements

For both the rough disks there was a small decrease in R_q over test stage 0 (the pre-conditioning). However, the scale of the decrease compared to that from the previous testing is small indicating only marginally more running-in. That there was any running-in at all can be attributed to the lubrication conditions of test stage 0 being more aggressive than any of those from previous testing. Critically, after test stage 0 there is no systematic variation in R_q (either increasing or decreasing) that might indicate significant wear: for test stages 1 to 5 the R_q of both disks remained within a range of ± 0.005 µm. The R_q of the smooth disks remained essentially constant throughout the experiments as anticipated. The ratio between the R_C of the rough and smooth disk pairs remained within a narrow range of 5.6 ± 0.2 throughout test stages 1 to 5 so that for an equivalent h_c, Λ was always ~ 5.6 times greater for the smooth disks compared to the rough disks.

To evaluate the stability of the rough disk surfaces the topographical history of the surface was examined by comparing the profiles measured at different times but in the same location. Figure 4 shows an example of this using a 0.3 mm length of the fast disk circumference. At most locations the profiles are all of similar shape, i.e. they overlay to form a single trace, indicating negligible wear. However at some locations the profiles are dissimilar, with some indicating the presence of an asperity and others a valley feature. This pattern is indicative of wear, specifically micro-pitting. Two prominent micro-pits are labelled in Figure 4. Sporadic micro-pit locations were found along all measured profiles from both disks. It is evident that micro-pitting occurred at some point during testing, but that it only

affected a small proportion of the total surface. The rate of micro-pitting is unknown, it may have occurred in a single test stage, or in all. A method for evaluating the rate of micro-pitting using in-situ 3D surface measurements is currently being developed by the authors. The implication of the micro-pitting on the lubrication conditions is discussed shortly in Section 3.3.

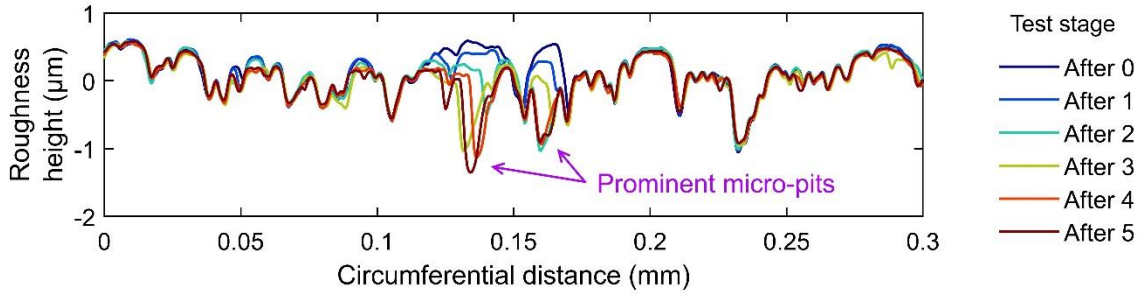

Figure 4. A short length of the rough fast disk roughness circumference showing profile measurments made at different times. The disk material is below the profiles.

The surface measurements serve to confirm and quantify two important conditions of the experiments, firstly, the stability of the rough surfaces, i.e. lack of any major wear, and secondly, the fundamental difference between the rough and smooth finishes.

3.2 Temperature, load and h_c

Figure 5 presents the temperatures, load and h_c for test stage one with the rough disks. As soon as the load was applied at time zero, the temperature of the disks quickly rose above that of the lubricant due to contact (frictional) heating. The slower response of the oil heater raised the lubricant temperature to match that of the disks within a few minutes and from this point on the increase in disk temperatures was driven primarily by oil heating. The rate of temperature increase reduced over the test stage as the rig radiated more heat (the oil heating was at constant power). At the end of the test stage the disk temperatures were approximately 10°C above that of the lubricant and this is explained by the continued but limited contribution of contact frictional heating. This pattern of heating was similar for all other test stages and both disk pairs.

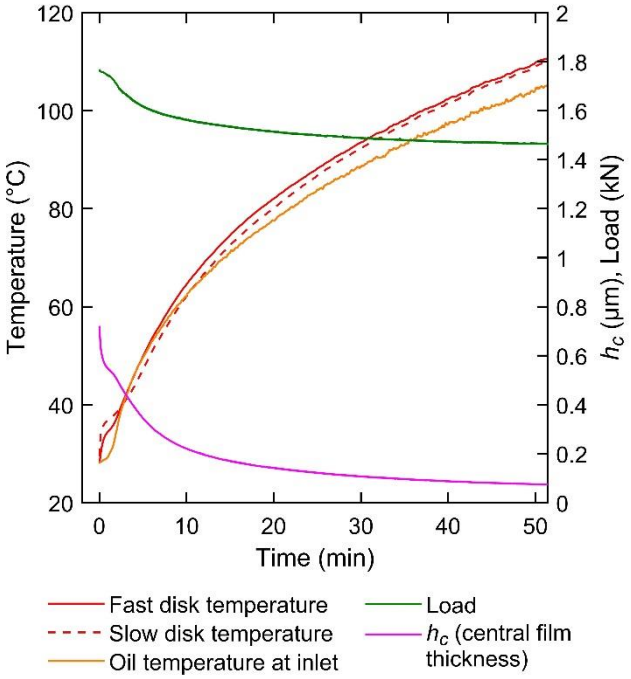

Figure 5. Temperatures, load, and h_c for test stage 1 of the rough disk pair.

Figure 5 shows that although the load was nominally specified as a constant it actually decreased slightly over the course of the test stage. This is because the hydraulic ram circuit takes oil from the lubricant tank and as the lubricant temperature increased the pressure supplied to the ram dropped. The instantaneous value of the load was used for calculating h_c (Equation 2). As the temperature profile was similar for all test stages and both disk pairs, so was the decrease in load. The total decrease in load corresponds to a 12% decrease in the width of the contact path (using Hertzian analysis).

For test stage one, h_c decreased by an order of magnitude from start to finish. This decrease occurred because of the substantial effects of temperature on the oil viscosity. The rate of decrease was highly non-linear in accordance with the rate of temperature rise. The form of the decrease in h_c was similar for all test stages, but had different values as the entrainment speed also has a strong effect on h_c. Table 4 shows the range of h_c for the rough disk tests, the ranges were similar for testing on the smooth disks.

Table 4. h_c ranges for the rough disk pair (all values rounded to 2 significant figures).

Test stage	Maximum h_c (μm)	Minimum h_c (μm)
1	0.70	0.074
2	1.1	0.10
3	1.8	0.16
4	2.4	0.20
5	3.0	0.25

3.3 Lambda

Table 5 shows the range of Λ for each test stage on the rough disks, from the maximum at the start when the oil was cold, to the minimum at the end when it was hot. It can be seen that for all test stages Λ dropped below unity, thus predicting with high likelihood that all stages generated mixed lubrication conditions at some point.

Also included in Table 5 is the ratio: $\Delta h_c/|\Delta R_C|$ calculated for each test stage. This is the ratio of the total change in h_c, and the total absolute change in R_C (the absolute value was used as for some test stages the change in R_C was negative). This gives an indication of the relative influence of changing film thickness and changing roughness on Λ. The values are all orders of magnitude above unity indicating that, as was hoped, the influence of changing roughness was negligible. It is concluded that any effect of wear on the lubrication conditions, including the limited micro-pitting (as shown in Figure 4) was insignificant in comparison with the relatively dramatic changes in film thickness.

Table 5. *Λ ranges for the rough disk pair (all values rounded to 2 significant figures).*

Test stage	Maximum Λ	Minimum Λ	$\Delta h_c/\|\Delta R_C\|$ (µm)
1	1.4	0.15	73
2	2.2	0.21	290
3	3.6	0.31	420
4	4.9	0.41	1700
5	6.0	0.49	540

3.4 Contact voltage

In this section Λ is referenced against the CV, a proven and direct measure of the amount / intensity of direct asperity contacts, in order to identify the range of Λ values that corresponded to mixed lubrication conditions.

Figure 6 presents the CVm (CV mean) vs. Λ for the rough disk pair. As the change in Λ over each individual test stage was continuous five curves are formed. Each can be read chronologically and in terms of increasing temperature from right to left.

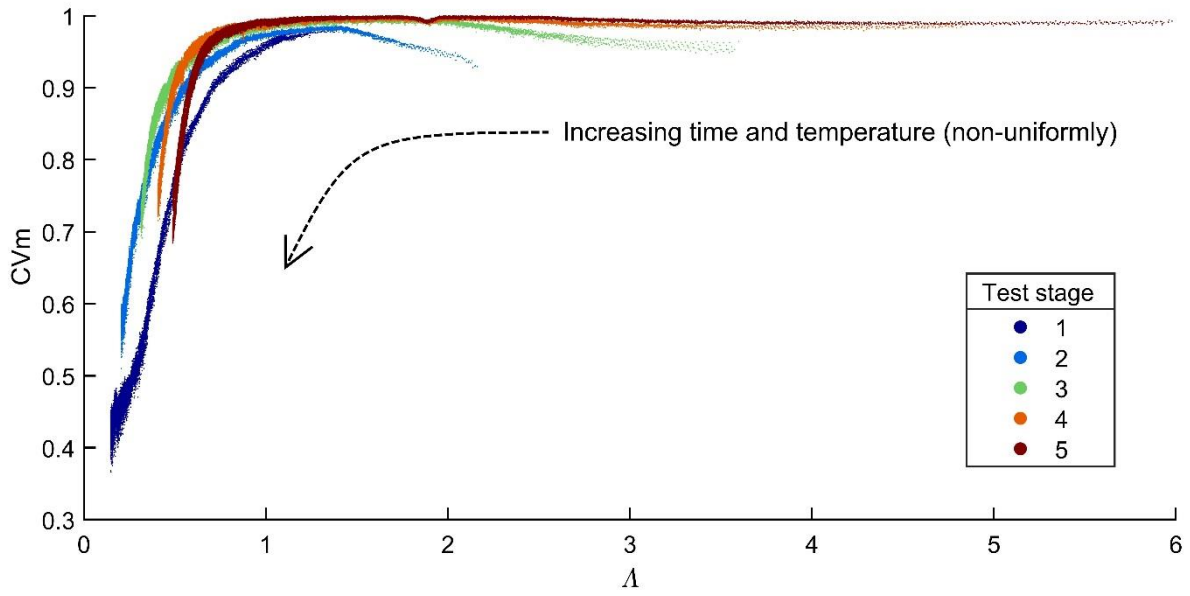

Figure 6. CVm vs. Λ for the rough disk pair.

The CVm measurements show that both full-film and the mixed lubrication conditions were tested, and clarifies the Λ range associated with each. As Λ drops from 6 to 1.5 the CVm remains broadly constant at its maximum indicating full-film lubrication, i.e. negligible direct asperity interactions. Below unity the CVm drops dramatically for all test stages indicating a transition to the mixed lubrication regime.

To verify that the drop in CVm was caused by increasing asperity contacts, the CVc (CV continuous) measurements were examined. Figure 7 shows the CVc vs. fast disk angular position vs. Λ. (The CVc signals from all the sampled fast disk rotations were sorted in order of Λ and stacked so as to be synchronised with the angular position of the fast disk). It can be seen that over the 90° of fast disk rotation shown, the CVc fluctuates rapidly between high and low values. There is a specific pattern of fluctuations, evident as horizontal banding, that cyclically repeats whilst slowly changing in intensity across the Λ range. (There is some waviness in the banding, but this is simply error in the measurement synchronisation). The cyclic nature of the CVc fluctuations helps to verify that the CV measurements are representative of changes in asperity contact. For example at approximately 57° there is a dark band that extends across almost the entire Λ range shown. This indicates a position on the fast and slow disks where one or more relatively aggressive and opposing asperities cyclically contact. In other positions the CVc measurements change over the test in accordance with the changing nominal Λ value. Other phenomena, such as debris passing through the contact and bridging the oil film, would not be expected to be synchronised with disk position in such a way. Previous experiments on the disk rig have established the repeatability of the CVc measurements in relation to the angular position of the disks [14].

.

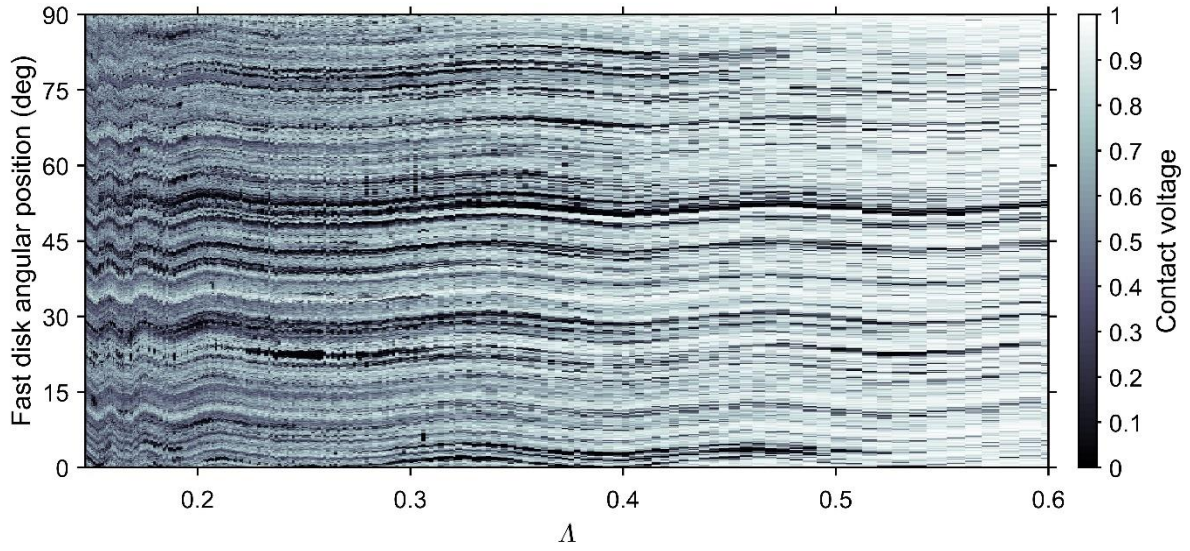

Figure 7. CVc vs. fast disk angular position vs. Λ for test stage one on the rough disk pair. For succintness only an arbitary 90° of fast disk rotation is shown and results at Λ greater than 0.6 have been omitted.

Regarding the smooth disk pair, the CVm measurements confirm that as expected the lubrication conditions barely entered the mixed regime. Figure 8 shows the CVm vs. h_c for both disk pairs. For the three fastest speeds on the smooth disks the CVm remained at unity over the entire decrease in h_c and so the curves are indistinguishable. For the slowest speed, the curve labelled A, the CVm did decrease at low h_c, indicating perhaps that some continued low level running-in was taking place, but despite this the CVm still indicates significantly fewer direct asperity interactions compared to the rough disks.

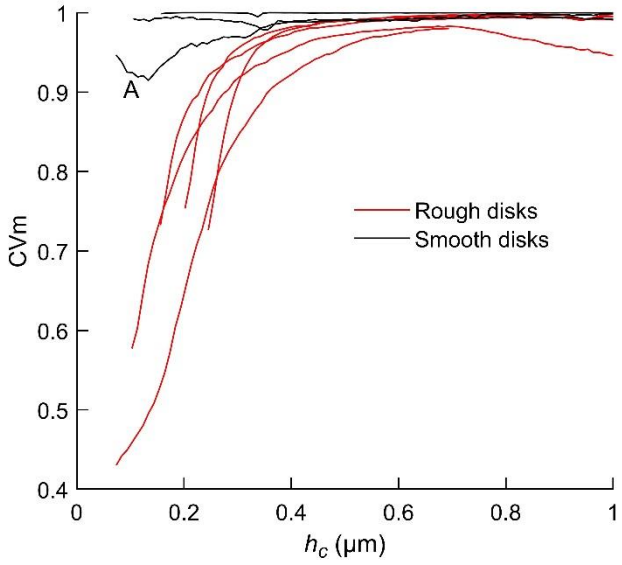

Figure 8. CVm vs. h_c for all test stages and both disk pairs. The curves have been filtered to reduce noise.

3.5 Acoustic emission from the rough disk pair

a) Identification of AE from asperity contacts

The broad characteristics of the AE measurements from the rough disks are now examined with the aid of Figure 9 which presents AE parameters vs. Λ for the 1st test stage (the slowest speed). For each AE sample, the parameters, which consist of RMS and FFT calculations, were calculated over their full length: a period of one fast disk rotation. This ensured that noise caused by rotational frequencies greater than that of the fast disk (e.g. the gear mesh frequenices) was filtered out.

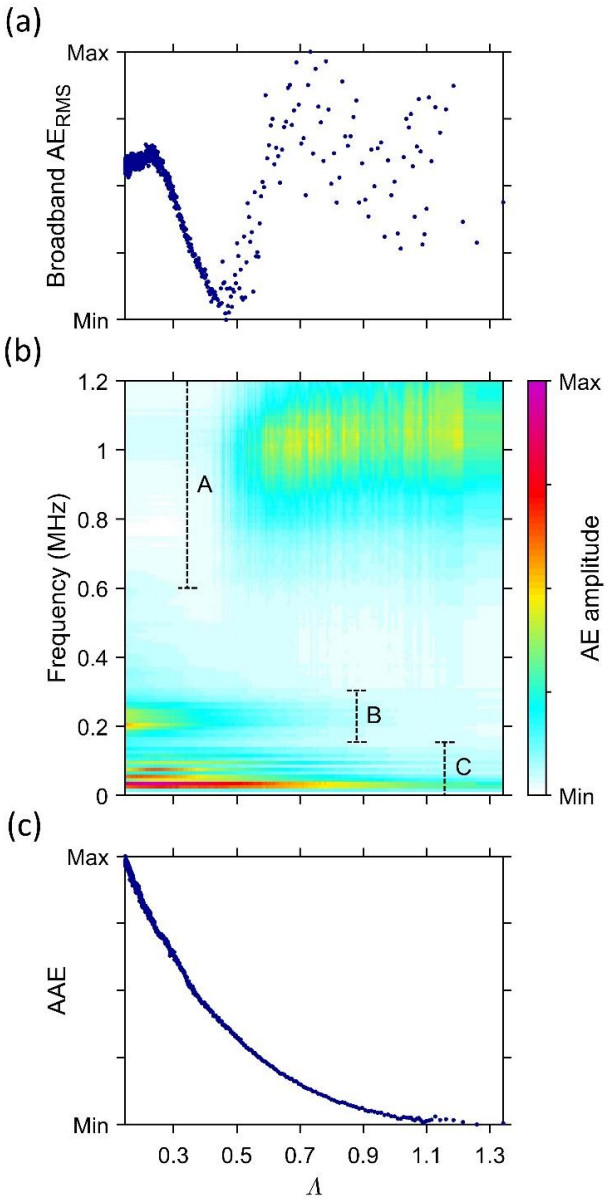

Figure 9. Various AE parameters vs. Λ for the 1st test stage and rough disks. The AE parameters are (a) the broadband RMS ampitude, (b) the binned frequency distribution (using 10 kHz wide bins), and (c) the AAE amplitude (RMS of the 150 - 300 kHz AE). All amplitudes are plotted on a linear scale between the minimum and maximum.

Figure 9 (a) shows the broadband AE_{RMS} vs. Λ. Over this test stage, the amount of asperity interactions increased continuously and monotonically with decreasing Λ, (as evidenced by the CV measurements) and therefore the amount of AAE is predicted to do likewise. Clearly the broadband AE_{RMS} does not, initially it has high scatter, it then becomes more precise whereupon it decreases, increases and then finally decreases again. The complexity of the broadband AE_{RMS} is due to conflict between AE of different frequencies. Figure 9 (b) shows the frequency distribution (in bins of 10 kHz) vs. Λ. There are three frequency ranges of significant and distinctly different AE behavour, these are labelled A, B and C. Range A is centred at approximately 1 MHz and the AE in this behaves entirely incongruously with the changing amount of asperity interactions: As Λ decreases towards a value of 0.5, activity in this range remains at a very noisy but constant amplitude after which it rapidly decays away. There are no easily identified characteristics of the test contact that might explain this change and so for the purposes of this paper it is treated as noise. Range B, defined as 150 – 300 kHz is the important range as far as these experiments are concerned. In this range the AE amplitude increases smoothly and continuously over the entire decrease in Λ. The form of the increase is also in accordance with the changing amount of asperity interactions, i.e. its rate of change also increases from high to low Λ. In the absence of any other obvious source of AE that might be expected to have a similar behavour it is concluded that range B consists primarily of AAE. The AAE parameter is thus defined here as the RMS of the 150 - 300 kHz AE, and Figure 9 (c) shows this vs. Λ. The AE in Range C, defined as 20 – 150 kHz, does behave partially in accordance with the changing amount of asperity interactions, however its increase is not as simple or consistent as that of range B. It is reasoned that there is at least some AE related to asperity interactions within range C, but since its relationship with Λ is not as clear as that from range B, it is not considered further.

b) The relationship between the AAE parameter and Λ.

The mathematical relationship between the AAE parameter and Λ is now examined in detail. As predicted, speed changes had a direct effect on the AAE and consequently the results from different speeds do not align in terms of their absolute values, i.e. at any constant Λ value the AAE in mV is different for each speed. Nevertheless there was consistency in the form of the relationship across all speeds. It was found that for every test stage the relationship could be described by the following general 'constant-speed' model:

$$AAE = Ae^{-B\Lambda} + C \tag{3}$$

where A, B and C are coefficients which are constant for a specific speed. Table 6 presents specific fits for each speed and Figure 10 shows the fits along with the measurements. Because the rate of change of Λ was highly non-linear with respect to time, (see the h_c profile in Figure 5), there were relatively few AAE samples at the high end of the Λ range for each test stage. To obtain good fits it was necessary to resample uniformly with respect to Λ and a smoothing spline interpolation was used to do this. The

amount of smoothing was chosen so that the spline faithfully followed the form of the original samples but also filtered out high frequency measurement noise. Table 6 also gives the coefficient of determination, R^2, for each fit between the constant-speed model and the resampled measurements. The R^2 values and Figure 10 show that the model accurately describes the relationship between Λ and the AAE parameter at all speeds tested.

Table 6. Specific fits of the constant-speed model.

Test stage	Mean entrainment speed $\bar{u}$ (m/s)	Coefficients (to 3 s.f.)			R^2
		A	B	C	
1	0.96	36.9	2.93	1.18	0.9996
2	1.60	84.3	2.76	2.79	0.9987
3	3.19	231	2.10	8.70	0.9996
4	4.79	375	1.83	21.6	0.9991
5	6.38	448	1.51	41.6	0.9972

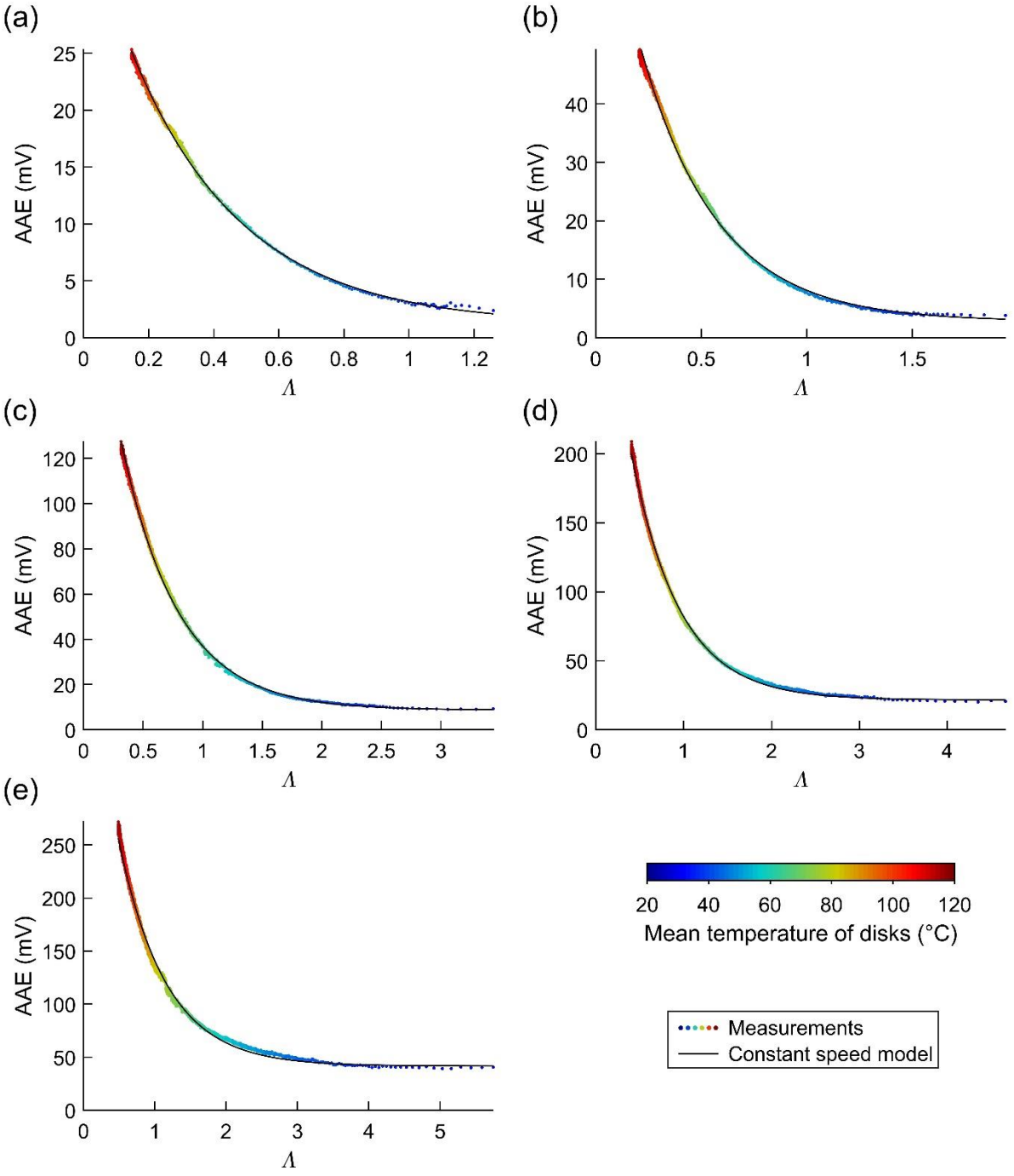

Figure 10. AAE parameter vs. Λ for the rough disk pair, showing both the measurements and fits of the constant speed model. (a) to (e) are test stages 1 to 5 respectively. The colour scale indicates the mean temperature of the disks.

The constant-speed model is composed of two terms, one a constant and the other an exponent, and together these describe the transition from full-film to mixed lubrication. At Λ values consistent with full-film conditions the exponential term becomes negligible and the remaining constant represents the background level of AE (in the 150 - 300 kHz range) that is unrelated to asperity interactions. As Λ

drops to mixed lubrication values the exponential term becomes significant and then dominant. It is this term which represents the increasing AAE.

c) The relationship between the AAE parameter, Λ and speed.

A model that incorporates the speed amplification is now presented. The five constant-speed fits in Table 6 show that *A*, *B* and *C* are functions of speed. Figure 11 (a) presents the variation of *A*, *B* and *C* with speed which is linear for *A* and *B* and has a power law form for *C*. Fits of the three relationships define the 'variable-speed' model, which is:

$$AAE = A(\bar{u})e^{-B(\bar{u})\lambda} + C(\bar{u}) \tag{4a}$$

where $\bar{u}$ is the mean entrainment speed and

$$A(\bar{u}) = 77.4\bar{u} - 29.9 \tag{4b}$$

$$B(\bar{u}) = -0.261\bar{u} + 3.12 \tag{4c}$$

$$C(\bar{u}) = 0.675\bar{u}^{2.20} \tag{4d}$$

The three fits, Equations 4 (b-d), are also plotted in Figure 11 (a). Figure 11 (b) presents a comparison of the AAE vs. Λ measurements, and the variable-speed model. The R^2 values for *A*, *B* and *C* are 0.987, 0.969 and 0.999, respectively. The error between the measurements and model is greater for the variable-speed model than the constant-speed models, and this is to be expected as it is more restrictive having 6 parameters rather than 15. The increased error occurs primarily because of apparent scatter in the linear relationships of A and B vs. speed.

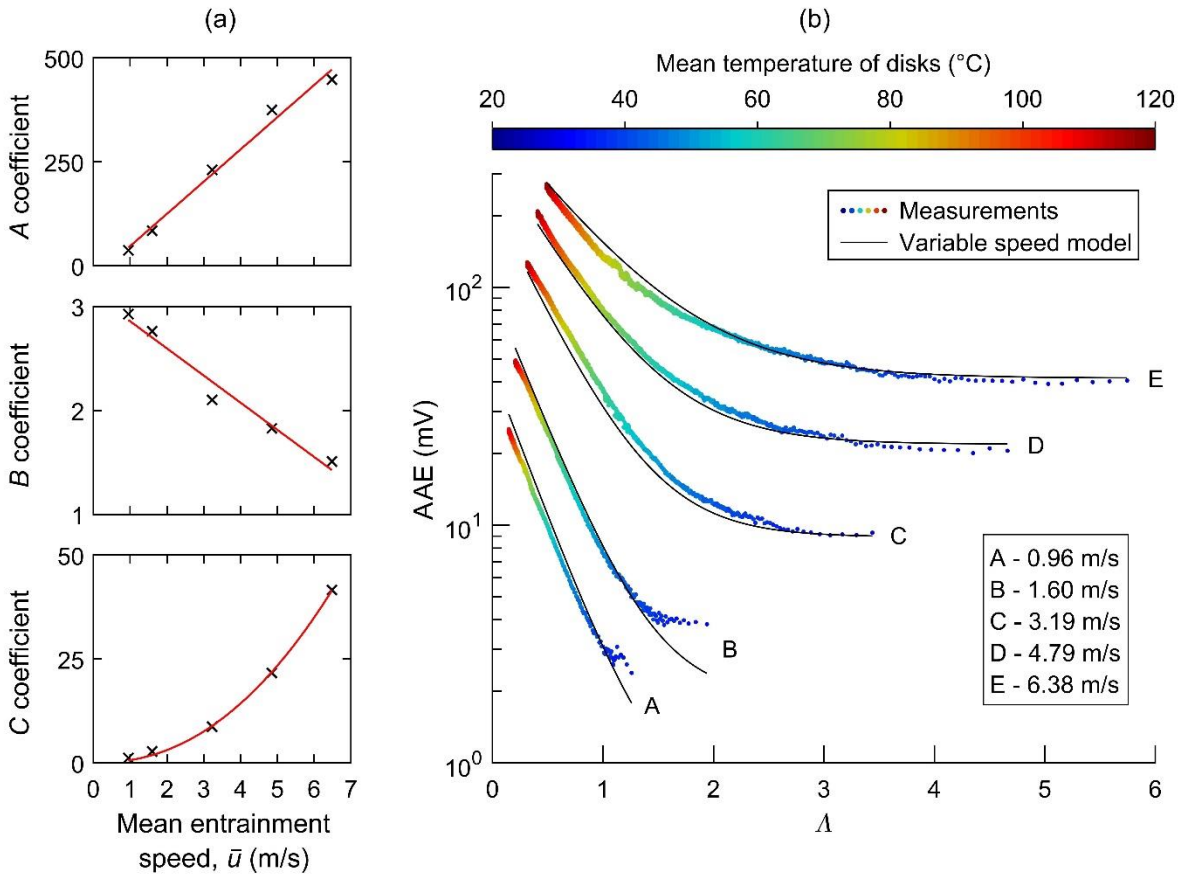

Figure 11. (a) The A, B and C coefficients from the constant-speed fits vs. $\bar{u}$, with the fits for the variable-speed model (Equations 4). (b) Semi-log plot of the AAE vs. Λ measurements and the variable speed model.

For the constant contact parameters of these experiments, the variable-speed model can be used to predict the AAE within the speed and Λ envelope tested. It is not yet known how changes to other common contact variables such as SRR and load may affect the relationship between AAE and Λ presented here, but this testing could easily be extended to include these as variables. With sufficient experimentation it should be possible to define a general relationship between AAE and Λ that covers most common operating conditions.

3.6 Comparison of the AE from the rough and smooth disk pairs.

Comparing the measurements obtained with the rough and smooth disks provides additional confirmation that the AAE (AE_{RMS} in the 150 to 300 kHz range) is caused by asperity interactions and not directly by the reducing film thickness or any other temperature effects. The CV measurements of Figure 8 show that the smooth disk pair did not enter, or barely entered, the mixed lubrication regime at low h_c. So for the smooth disk pair there should be no, or minimal, increase in the AAE and Figure 12, which presents the AAE vs. h_c for both disk pairs and all test speeds, shows this to be the case. As h_c decreases below 0.5 μm, (which is approximately equivalent to a Λ of unity for the rough disks and Λ of 5.6 for the smooth), the AAE increases exponentially for the rough disks but remains at a low level

and actually decreases slightly for the smooth disks. This clearly demonstrates that the AAE has been identified correctly.

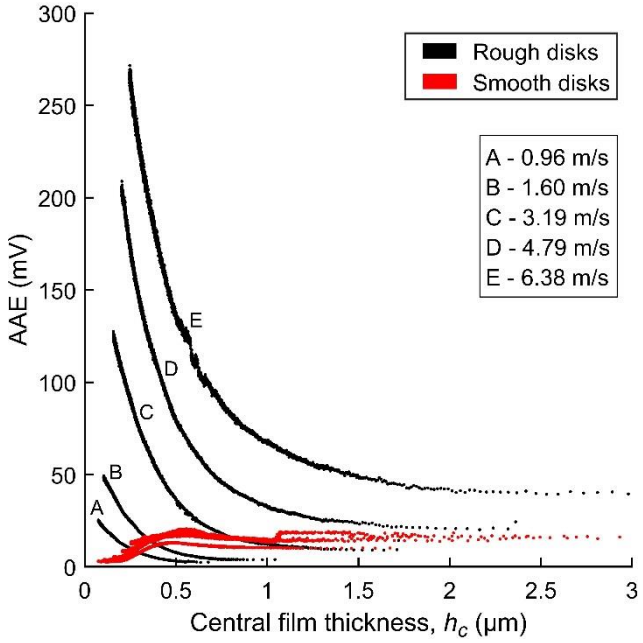

Figure 12. The AAE parameter vs. Central film thickness, h_c for both disk pairs and all test speeds.

4 Conclusions

The experiments presented in this paper demonstrate with improved clarity and certainty that asperity interactions in mixed lubrication gear contacts cause predictable AE. It was found that:

- An AE parameter, the RMS of the 150 - 300 kHz AE signal and termed here the AAE, varies in accordance with the amount of asperity contacts as predicted by the Λ range and verified using contact voltage measurements.

- In full film conditions the AAE remains at a relatively constant background level irrespective of decreasing oil film thickness. However, in mixed lubrication the AEE increases exponentially with decreasing oil film thickness, the result of increasing asperity contacts.

- Within the range of parameters tested, and at constant speed, the AAE corresponding to a particular value of Λ can be accurately predicted using a simple two-term model.

- Increases in speed directly increase the AE amplitude independently of any effects on the amount of asperity contact. Within the parameters of these experiments is it possible to predict the AEE at intermediate speeds using a model that incorporates the speed as a variable.

This research shows that AAE measurements can indicate the change from full-film to mixed lubrication conditions, and even subtle changes within the mixed lubrication spectrum. This is clearly of considerable interest for lubrication monitoring of gears, and other heavily loaded EHL contacts.

Data Access Statement

Information on how to access the data that supports the results presented in this article can be found in the Cardiff University data catalogue at http://dx.doi.org/10.17035/d.2016.0008118727.

Acknowledgements

The authors wish to acknowledge the support of EPSRC (Grant reference EP/L021757/1) which supported this work in part, together with REM Surface Engineering Ltd who kindly superfinished test samples.

References

[1] Grosse C.U., Ohtsu M., 2008, *Acoustic emission testing*, Berlin, Heidelberg: Springer-Verlag.

[2] Tandon N., Mata S., 1998, Detection of defects in gears by acoustic emission measurements, *Journal of Acoustic Emission*, vol. 17, pp. 23–7.

[3] Loutas T., Sotiriades G., et al., 2009, Condition monitoring of a single-stage gearbox with artificially induced gear cracks utilizing on-line vibration and acoustic emission measurements, *Applied Acoustics*, vol. 70, pp. 1148–59.

[4] Loutas T.H., Roulias D., et al., 2011, The combined use of vibration, acoustic emission and oil debris on-line monitoring towards a more effective condition monitoring of rotating machinery, *Mechanical Systems and Signal Processing*, vol. 25, pp. 1339–52.

[5] Qu Y., He D., et al., 2014, Gearbox tooth cut fault diagnostics using acoustic emission and vibration sensors--a comparative study, *Sensors*, vol. 14, pp. 1372–93.

[6] Asamene K., Sundaresan M., 2012, Analysis of experimentally generated friction related acoustic emission signals, *Wear*, vol. 296, pp. 607–18.

[7] Hase A., Mishina H., Wada M., 2012, Correlation between features of acoustic emission signals and mechanical wear mechanisms, *Wear*, vol. 292–293, pp. 144–50.

[8] Benabdallah H.S., Aguilar D.A., 2008, Acoustic emission and its relationship with friction and

wear for sliding contact, *Tribology Transactions*, vol. 51, pp. 738–47.

[9] Snidle R.W., Evans H.P., et al., 2003, Understanding Scuffing and Micropitting of Gears. *Control Reduct. Wear Mil. Platforms*, June, pp. 7–9.

[10] Oila A., Bull S.J., 2005, Assessment of the factors influencing micropitting in rolling/sliding contacts, *Wear*, vol. 258, pp. 1510–24.

[11] Tallian T.E., 1967, On competing failure modes in rolling contact, *A S L E Transactions*, vol. 10, pp. 418–39.

[12] Krantz T.L., 2015, On the Correlation of Specific Film Thickness and Gear Pitting Life, *Gear Technology*, February, pp. 52–62.

[13] Šperka P., Křupka I., Hartl M., 2012, The behavior of surface roughness in EHL contacts under small slide to roll ratios, *Tribology Letters*, vol. 47, pp. 357–66.

[14] Clarke A., Weeks I.J.J., et al., 2016, An investigation into mixed lubrication conditions using electrical contact resistance techniques, *Tribology International*, vol. 93, pp. 709–16.

[15] Novoa A.B., Vicuña C.M., 2016, New aspects concerning the generation of acoustic emissions in spur gears, the influence of operating conditions and gear defects in planetary gearboxes, *Insight - Non-Destructive Testing and Condition Monitoring*, vol. 58, pp. 18–27.

[16] Raja Hamzah R.I., Mba D., 2009, The influence of operating condition on acoustic emission (AE) generation during meshing of helical and spur gear, *Tribology International*, vol. 42, pp. 3–14.

[17] Tan C.K., Mba D., 2005, Experimentally established correlation between acoustic emission activity, load, speed, and asperity contact of spur gears under partial elastohydrodynamic lubrication, *Proceedings of the Institution of Mechanical Engineers, Part J: Journal of Engineering Tribology*, vol. 219, pp. 401–9.

[18] Raja Hamzah R.I., Al-Balushi K.R., Mba D., 2008, Observations of acoustic emission under conditions of varying specific film thickness for meshing spur and helical gears, *Journal of Tribology*, vol. 130, pp. 021506 1-12.

[19] Vicuña C.M., 2014, Effects of operating conditions on the Acoustic Emissions (AE) from planetary gearboxes, *Applied Acoustics*, vol. 77, pp. 150–8.

[20] Mirhadizadeh S.A., Mba D., 2009, Observations of acoustic emission in a hydrodynamic

bearing, *Journal of Quality in Maintenance Engineering*, vol. 15, pp. 193–201.

[21] Cockerill A., Clarke A., et al., 2016, Determination of rolling element bearing condition via acoustic emission, *Proceedings of the Institution of Mechanical Engineers, Part J: Journal of Engineering Tribology,* vol. 230, pp. 1377–88.

[22] Merritt H.E., 1962, Gear-tooth contact phenomena, *Proceedings of the Institution of Mechanical Engineers*, vol. 176, pp. 141–63.

[23] Defence Procurement Agency, 2006, Defence Standard 91-74, Lubricating Oil, Steam Turbine and Gear, Extreme Pressure Joint Service Designation: OEP-80.

[24] Patching M.J., Kweh C.C., et al., 1995, Conditions for scuffing failure of ground and superfinished steel disks at high sliding speeds using a gas turbine engine oil, *Journal of Tribology*, vol. 117, pp. 482-9.

[25] Hutt S., Clarke A., Evans H.P., 2018, Generation of Acoustic Emission from the running-in and subsequent micropitting of a mixed-elastohydrodynamic contact, *Tribology International*, vol. 119, pp. 270–80.

[26] Konstantinidis G., Wilcox P.D., Drinkwater B.W., 2007, An investigation into the temperature stability of a guided wave structural health monitoring system using permanently attached sensors, *IEEE Sensors Journal*, vol. 7, pp. 905–12.

[27] Chittenden R.., Dowson D., et al., 1985, A theroretical analysis of the isothermal elastohydrodynamic lubrication of concentrated contacts II general case, with lubricant entrainment along either principal axis of the Hertzian contact ellipse or at some intermediate angle, *Proceedings of the Royal Society of London A*, vol. 397, pp. 271–94.